

镁/钛异种金属冷金属过渡焊接的温度场模拟

王 岑¹, 曹 睿¹, 林巧力¹, 王 清², 董 闯², 陈剑虹¹

(1. 兰州理工大学 有色金属先进加工与再利用省部共建国家重点实验室, 兰州 730050;

2. 大连理工大学 三束材料改性教育部重点实验室, 大连 116024)

摘 要: 利用 ABAQUS 有限元软件建立镁/钛异种金属搭接接头的有限元模型, 对镁/钛异种金属冷金属过渡焊接过程的温度场进行模拟, 分析温度场的变化规律, 并通过试验验证模拟结果的准确性. 比较了不同送丝速度下温度场的变化规律, 并对特征点的显微组织进行比较. 结果表明, 镁、钛两侧的温度场呈不对称分布. 距离焊缝中心相同的两点, 镁板侧试件温度上升较快, 达到的峰值温度比钛板侧高, 且下降速度也快. 随着送丝速度的增加, 峰值温度变高, 达到钛板的熔化温度, 钛的熔化量也就随之增加. 镁钛连接界面有较好的结合.

关键词: 镁/钛异种金属; 冷金属过渡; 焊接温度场; 数值模拟

中图分类号: TG 402 文献标识码: A 文章编号: 0253-360X(2015)04-0017-04

0 序 言

镁合金是目前可应用的最轻的结构材料, 具有比强度和比刚度高、导热导电性能好、阻尼减震性和电磁屏蔽性强、易加工成形、废料易回收等特点^[1]. 钛及钛合金被称为 21 世纪的绿色金属材料, 具有密度小、比强度高、塑性韧性好、耐热性耐蚀性好、可加工性好等特点^[2]. 钛合金与镁合金异种材料的有效连接可以充分发挥镁合金和钛合金材料的性能优势, 达到“物尽其用”的效果.

然而镁、钛两种金属性能相差很大^[3], 使得两种金属焊接性较差, 造成焊接缺陷, 这些都与焊接热循环过程息息相关. 因此, 对镁/钛异种金属焊接过程的研究具有重要意义. 冷金属过渡技术 (cold metal transfer, CMT) 具有热输入量小; 无飞溅起弧, 减少焊后清理工作等优点^[4]. 文中在王涛等人^[5]研究的基础上, 运用 ABAQUS 有限元软件对 AZ31B 镁合金和 TA2 纯钛异种金属 CMT 焊接过程进行研究, 考虑焊缝对温度的影响, 利用单元生死技术模拟焊缝的填充过程, 并对模拟结果进行试验验证. 最后, 通过模拟不同工艺参数下温度场的分布, 进一步说明温度对镁、钛异种金属连接的影响.

1 试验方法

试验选用尺寸为 200 mm × 50 mm × 1 mm 的

AZ31B 镁合金和 TA2 纯钛, 以及直径为 1.2 mm 的 AZ61 镁合金焊丝. 采用奥地利 Fronius 公司生产 TPS-3200 系列数字化 CMT 焊机进行钛板在上, 镁板在下的搭接焊, 搭接宽度为 10 mm, 如图 1 所示. 焊接过程中, 根据焊接参数的不同, 焊丝在钛板上有一定的偏移量, 这样才能保证有较好的焊缝成形和较好力学性能的镁/钛焊接接头^[5].

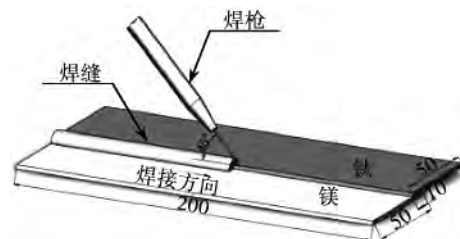


图 1 镁/钛异种金属 CMT 焊接示意图 (mm)

Fig. 1 Schematic diagram of CMT welding Mg/Ti dissimilar alloys

焊接过程采用 99.99% 氩气保护, 流量为 15 L/min, 焊接工艺参数见表 1. 焊接速度为 10 mm/s 不变, 研究不同送丝速度下焊接温度场的变化.

表 1 焊接工艺参数

Table 1 Welding parameter

送丝速度 $v_f / (\text{m} \cdot \text{min}^{-1})$	焊接速度 $v / (\text{mm} \cdot \text{s}^{-1})$	焊接电流 I / A	焊接电压 U / V
9.5	10	110	10.5
11.5	10	145	12.0

收稿日期: 2013-10-08

基金项目: 国家自然科学基金资助项目 (51265028); 三束材料改性教育部重点实验室 (大连理工大学) 开放课题 (LABKF1402)

2 有限元模型建立

2.1 有限元模型

运用 ABAQUS 有限元软件建立一个三维 (3D) 有限元模型并运用 Fortran 语言编写*DFLUX 子程序,实现热源的加载过程.根据 CMT 焊接镁钛时的焊缝形貌选用双椭球体热源模型^[6],其形状、尺寸与实际情况较符合,热流密度 q 按高斯函数正态分布,其前后两部分表达式不同,前半部分表达式为

$$q_f(x, y, z) = \frac{6\sqrt{3}(f_f Q)}{a_f b_f c_f \pi \sqrt{\pi}} \left(-\frac{3x^2}{a_f^2} - \frac{3y^2}{b_f^2} - \frac{3z^2}{c_f^2} \right), x \geq 0$$

后半部分表达式为

$$q_r(x, y, z) = \frac{6\sqrt{3}(f_r Q)}{a_r b_r c_r \pi \sqrt{\pi}} \left(-\frac{3x^2}{a_r^2} - \frac{3y^2}{b_r^2} - \frac{3z^2}{c_r^2} \right), x < 0$$

式中: $Q = \eta UI$, 其中 η 为热源效率; U 为焊接电压 (V); I 为焊接电流,焊接电流和焊接电压取自 CMT 焊接时记录的对应值; a_f, b_f, c_f 为椭球形状参数; f_f, f_r 为前后椭球热量分布函数 $f_f + f_r = 2$.

由于焊接是一个不均匀的加热过程,在焊缝及其热影响区温度梯度变化较大,因此采取不均匀的网格,在焊缝及近缝区采用较细的网格;而在远离焊缝区,采用相对稀疏的网格^[7].此温度场求解时采用的网格类型是 DC3D8,单元个数为 48 000 个.有限元网格划分如图 2 所示.计算时,考虑焊缝金属的填充过程,运用单元生死技术,在一开始将焊缝金属移除,当焊缝经过每一单元时,再将单元逐一激活,材料参数恢复到设置的值.



图 2 有限元网格划分
Fig. 2 FEM mesh generation

2.2 材料物理性能

随着温度的升高,材料的物理性能也随之改变.模拟过程中认为镁焊丝的物理性能与镁母材相同.高温时的物理性能由外推法^[8]获得.在模拟过程中不考虑相变潜热对温度的影响.

2.3 边界条件

由于在焊件背面加有垫板,因此在材料的背面加一个强制对流,这对试件冷却过程非常重要.表面对流和辐射边界条件表达为

$$k \frac{\partial T}{\partial n} = \alpha (T - T_0)$$

式中: T 为材料温度; n 为法向方向单位矢量; K 为热导率; α 为总换热系数; T_0 为初始温度.计算时定义初始温度为室温 (27 °C),辐射发射率为 0.8^[9],试件底部以外的对流系数为 10 W/m²K.

3 模拟结果与分析

3.1 送丝速度为 11.5 m/min 时的温度场分析

3.1.1 温度场分布云图

图 3 为送丝速度为 11.5 m/min 时,不同时刻温度场的分布云图.图 3 中左侧为 TA2 纯钛,右侧为 AZ31B 镁合金.图 3a, b, c 为施焊过程的温度分布,图 3d 为焊接结束冷却过程的温度分布.从图 3 中可以看出,随着热源移动,熔池向前推进,熔池形貌基本不变,这就说明焊接过程相对比较稳定.由于焊缝两侧为两种不同的金属,且钛板与镁合金之间的物理性能相差较大,所以云图中的等温线分布是不对称的.由于钛的热导率较镁小很多,所以钛侧冷却速度慢.同时,从云图中可以看出,钛侧的温度梯度相对镁侧较小.从图 3d 中 22 s 时的温度分布可以看出,钛侧的冷却速度较镁侧慢.

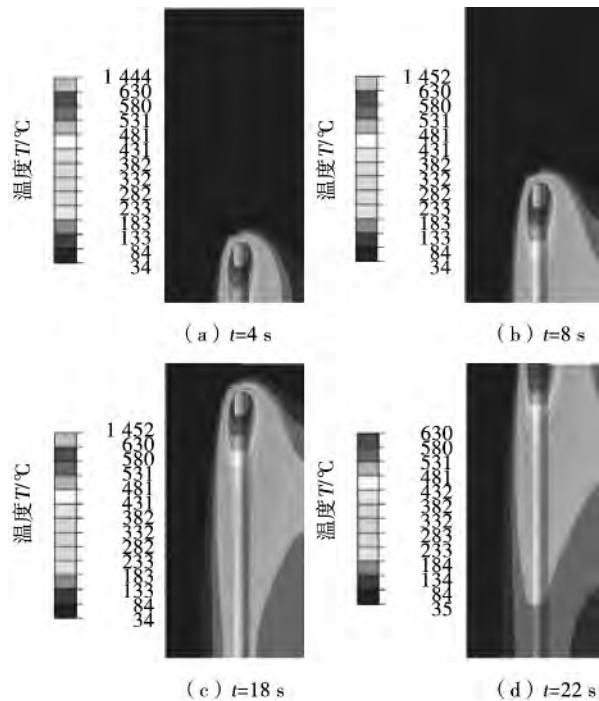


图 3 不同时刻温度场分布云图

Fig. 3 Contours of temperature field distribution in different time

在钛板和镁板上分别选取一些特征点进行温度场测试,如图 4b 所示,图中 F, G 点分别为位于钛板和镁板上表面,且距焊缝中心的距离均为 10 mm.

图5为图4b中F、G两点热循环曲线比较,从图5中可以看出,F点在12.98 s时达到峰值,峰值温度为380 °C,再经过28.6 s冷却到100 °C,G点11.37 s达到峰值484 °C,再经过27.4 s降到100 °C。可以看出,焊缝中心相同距离的两点,镁板侧试件温度上升较快,达到的峰值温度比钛板侧高,且下降速度也稍快。这是因为,镁合金与钛相比虽然具有较大的比热容,但是镁合金有较大的热导率,且具有较小的密度。

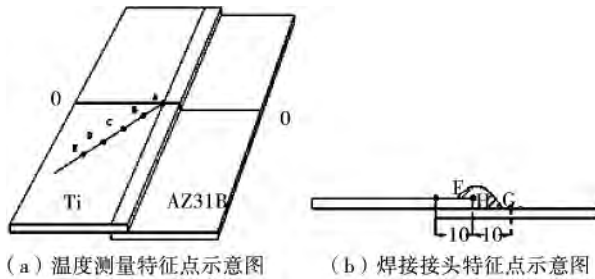


图4 特征点示意图(mm)
Fig. 4 Schematic diagram of feature points

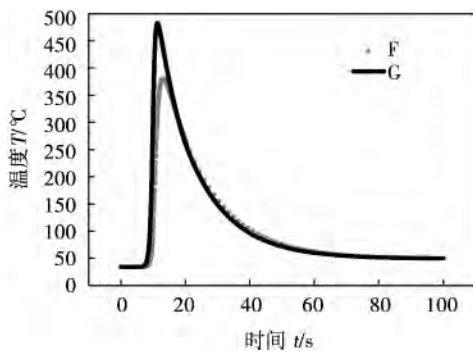


图5 特征点热循环曲线对比
Fig. 5 Comparison between thermal cycle curves at feature points

3.1.2 试验验证

为了验证模拟的准确性,对焊接过程中特征点处的温度进行测量,特征点如图4a所示。在钛板上表面测量斜45°线上A、B、C、D、E的五个点,测量时选用K型热电偶。将试验测得结果与模拟结果进行对比,如图6所示。可以看出,试验测得特征点热循环曲线与计算结果基本吻合,由于计算过程中存在各种假设,以及试验测量过程中的误差,导致计算结果与试验结果会有一些的偏差,但这种偏差是可以接受的。

3.2 工艺参数对温度场的影响

通过试验验证,证明计算结果的准确性。图7为不同送丝速度下焊接8 s时的横截面温度分布云

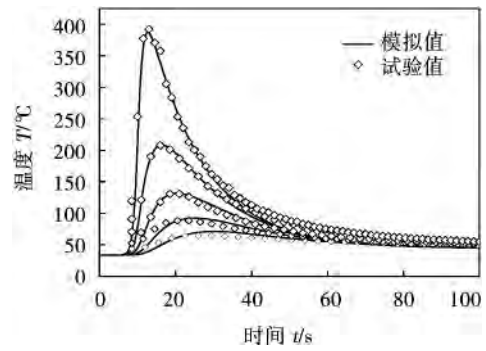


图6 试验与模拟特征点热循环曲线的对比
Fig. 6 Comparison of thermal cycle curves between numerical and experimental results at feature points

图。可以看出,送丝速度为11.5 m/min时的峰值温度比9.5 m/min时高出317 °C,且上表面及下表面的熔化宽度也明显增大。取钛板边缘H点(图4b),对该点不同送丝速度的热循环曲线进行对比,如图8所示。图8中两个参数的热循环曲线趋势基本一致。送丝速度为11.5 m/min时的峰值温度为1 030 °C,比送丝速度为9.5 m/min时高230 °C。这是因为送丝速度增大,焊丝的熔化量增大,在焊接速度不变的情况下焊接线能量是增大的。随着焊接线能量的增加,熔池温度也随之升高。

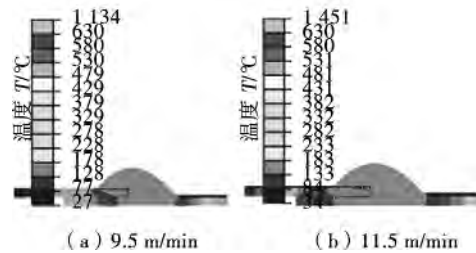


图7 不同送丝速度时焊缝横截面温度分布
Fig. 7 Temperature distributions of cross section at different wire feed speeds

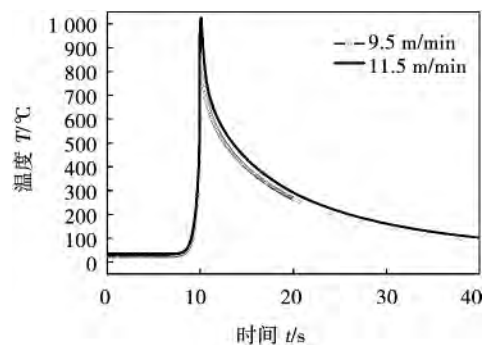
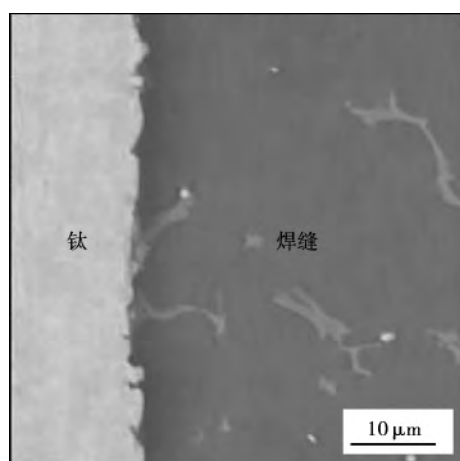
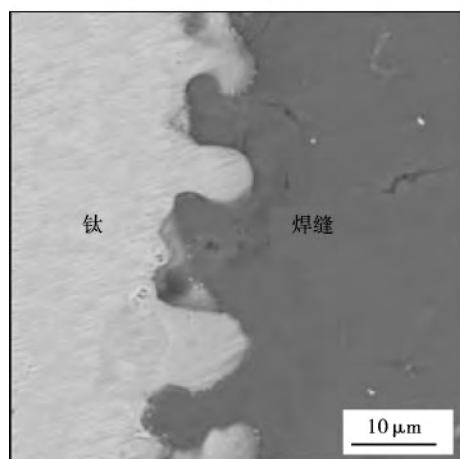


图8 不同送丝速度时图4b中H点的热循环曲线对比
Fig. 8 Thermal cycle curves comparison of point H in Fig. 4b at various wire feed speeds

图 9 为不同送丝速度时图 4b 中 H 点的显微组织形貌, 送丝速度为 9.5 m/min 时钛基本没有熔化, 也没有向镁侧扩散, 是因为送丝速度小, 焊接热输入小, 导致温度较低, 没有达到钛的熔化温度. 而送丝速度为 11.5 m/min 时明显看出钛板局部熔化, 这说明随着焊接热输入的增加, 达到钛的熔化温度, 从而使钛的反应量增多^[5]. 图 9 界面显微组织图与图 7 中模拟的结果吻合. 由于镁钛之间固溶度很小, 且没有金属间化合物生成, 要使这两种金属实现较好的连接, 必须通过增加焊接热输入以及调整合适的焊丝偏移量, 使钛侧熔化量增加的同时得到好的焊缝成型和力学性能.



(a) 9.5 m/min



(b) 11.5 m/min

图 9 图 4b 中 H 点显微组织形貌

Fig. 9 Microstructure morphology of point H in Fig. 4b

4 结 论

(1) 镁/钛异种金属 CMT 温度场模拟表明, 镁、钛两侧的温度场呈不对称分布. 距离焊缝中心相同的两点, 镁板侧试件温度上升较快, 达到的峰值温度

比钛板侧高, 且下降速度也快.

(2) 采用热电偶对焊接过程特征点的热循环曲线进行测量, 测量结果与计算结果基本吻合, 验证了模拟的准确性.

(3) 对不同工艺参数的温度场分析表明, 随着送丝速度增大, 焊缝横截面上下表面熔化宽度增大, 特征点的热循环曲线的峰值温度也随之升高.

(4) 从界面处的显微组织可以看出, 送丝速度越大, 界面处钛的反应量越多, 镁钛结合界面越致密.

参考文献:

- [1] 曾荣昌, 柯伟, 徐永波, 等. Mg 合金的最新发展及应用前景[J]. 金属学报, 2001, 37(7): 672-685.
Zeng Rongchang, Ke Wei, Xu Yongbo, et al. Recent development and application of magnesium alloys[J]. Acta Metallurgica Sinica, 2001, 37(7): 672-685.
- [2] Leyens C, Peters M. Titanium and titanium alloy[M]. Wiley Online Library, 2003.
- [3] 熊江涛, 张赋升, 李京龙, 等. 镁合金与钛合金的瞬间液相扩散焊[J]. 稀有金属材料与工程, 2006, 35(10): 1677-1680.
Xiong Jiangtao, Zhang Fusheng, Li Jinglong, et al. Transient liquid phase bonding of magnesium alloy (AZ31B) and titanium alloy (Ti6Al4V) using aluminum interlayer[J]. Rare Metal Materials and Engineering, 2006, 35(10): 1677-1680.
- [4] 杨修荣. 超薄板的 CMT 冷金属过渡技术[J]. 焊接, 2005(12): 52-64.
Yang Xiurong. CMT technic of the ultrathin sheets[J]. Welding & Joining, 2005(12): 52-64.
- [5] 王涛, 曹睿, 陈剑虹, 等. 镁和钛异种金属冷金属过渡焊接接头微观组织及力学性能的分析[J]. 机械工程学报, 2014, 50(4): 75-79.
Wang Tao, Cao Rui, Chen Jianhong, et al. Analysis of microstructure and mechanical properties for welding joints of dissimilar metals between magnesium and titanium by cold metal transfer method[J]. Journal of Mechanical Engineering, 2014, 50(4): 75-79.
- [6] Zeng Zhi, Li Xunbo, Miao Yugang, et al. Numerical and experiment analysis of residual stress on magnesium alloy and steel butt joint by hybrid laser-TIG Welding[J]. Computational Materials Science, 2011, 50: 1763-1769.
- [7] Chen Shuhai, Li Liqun, Chen Yanbin, et al. Improving interfacial reaction nonhomogeneity during laser welding-brazing aluminum to titanium[J]. Materials and Design, 2011, 32: 4408-4416.
- [8] 段潇恢. 钛/钢异种金属电子束焊接温度场与应力场模拟研究[D]. 哈尔滨: 哈尔滨工业大学, 2011.
- [9] 方洪渊. 焊接结构学[M]. 北京: 机械工业出版社, 2008.

作者简介: 王岑, 女, 1988 年出生, 硕士研究生. 主要研究方向为异种金属焊接的数值模拟. 发表论文 1 篇. Email: wangcen@126.com

通讯作者: 曹睿, 女, 教授, 博士研究生导师. Email: caorui@lut.cn

sum of root face and misalignment was less than 4 mm , the weld with good root fusion could be obtained with reserved 2-4 mm groove gap. When the sum of root face and misalignment was more than 6 mm , incomplete penetration occurred. When the sum was between 4 mm and 6 mm , the root fusion changed with the reserved groove gap.

Key words: double-sided TIG backing welding; root fusion; numerical simulation of temperature field

Numerical simulation on temperature distribution of cold metal transfer joining magnesium to titanium dissimilar metals

WANG Cen¹ , CAO Rui¹ , LIN Qiaoli¹ , WANG Qing² , DONG Chuang² , CHEN Jianhong¹ (1. State Key Laboratory of Advanced Processing and Recycling of Non-ferrous Metal , Lanzhou University of Technology , Lanzhou 730050 , China; 2. Key Laboratory of Materials Modification by Laser , Ion and Electron Beams , Ministry of Education , Dalian University of Technology , Dalian 116024 , China). pp 17 - 20

Abstract: Using ABAQUS finite element software , a finite element model was established on magnesium/titanium dissimilar metal cold metal transfer lap joint to numerically simulate the temperature distribution. The simulated temperature field was verified by experimental results. The variation of temperature field and microstructure at specified location of the joint were compared at different wire feed speeds. The results show that the distribution of temperature field was asymmetric on magnesium and titanium sides. At two locations with the same distance from the weld center , the temperature rose rapidly on magnesium side , a higher peak temperature in Mg sheet was reached than that in Ti sheet , and the rate of decline was also fast. As the wire feed speed increased , the peak temperature became higher and reached the molten temperature of titanium sheet , then the amount of molten Ti increased , finally sound Mg/Ti interface formed.

Key words: Mg/Ti dissimilar metals; cold metal transfer; welding temperature field; numerical simulation

Electromigration failure of Al-Si interconnects CUI Hai-po , DENG Deng (Shanghai Institute for Minimally Invasive Therapy , University of Shanghai for Science and Technology , Shanghai 200093 , China). pp 21 - 24

Abstract: With development of microelectronics technology , the cross-sectional area of metal film used in very large scale integrated circuit interconnects are getting smaller and smaller , causing a sharp increase in its exposure of current density. Interconnects failure induced by electromigration has become particularly prominent. In accordance with the electromigration of metal interconnects in integrated circuits , the Black equation was modified. The electromigration of Al-Si interconnects was investigated by accelerated life time test. The relevant parameters of modified Black equation were obtained. The influence of test temperature , current density , initial resistance on the electromigration of Al-Si interconnects were analyzed. The results indicate that

the electromigration life of Al-Si interconnects is inversely proportional to those parameters.

Key words: electromigration; accelerated life time test; interconnect

Prediction of fatigue life of titanium alloy welded joints based on RS_RBFNN

ZOU Li¹ , YANG Xinhua² , SUN Yibo² , DENG Wu^{1,3} (1. Software Institute , Dalian Jiaotong University , Lvshun 116052 , China; 2. School of Materials Science and Engineering , Dalian Jiaotong University , Dalian 116028; 3. Chongqing Key Laboratory of Computational Intelligence , Chongqing 400065 , China). pp 25 - 29 , 78

Abstract: An integrated model of rough set and neural network (RS_RBFNN) was proposed for predicting fatigue life of titanium alloy welded joints. The fatigue data were discretized by using the entropy-based algorithm , and the fatigue evaluation indices were reduced without information loss through a genetic algorithm. The reduced indices were used to develop the rules for fatigue life of welded joints and to train the RBF neural network. The rough set theory was used to determine the category of fatigue life for the test samples which matched the rules in the rule-base. The neural network was applied to those test samples which did not match any rules in the rule-base. Experimental results based on the fatigue data of titanium alloy show that the RS_RBFNN model for fatigue analysis of welded joints had improved fault tolerance and precision. Therefore this model is of practical significance for predicting fatigue life of titanium alloy welded joints.

Key words: rough set; neural network; welding; fatigue

Numerical simulation of influence of ultrasonic impact treatment on welding stress of 7A52 aluminum alloy joint

JIA Cuiling^{1,2} , CHEN Furong¹ (1. Institution of Materials Science and Engineering , Inner Mongolia University of Technology , Hohhot 010051 , China; 2. Engineering Training Center , Inner Mongolia University of Technology , Hohhot 010051 , China). pp 30 - 34

Abstract: A thermal coupling numerical model was established for double-wire MIG welding of 7A52 aluminum alloy , based on the finite element software ABAQUS , and the welding residual stress field was obtained. A coupling model of ultrasonic impact treatment on the welded joint was built with numerical method and the residual stress field was obtained after ultrasonic impact treatment. The distribution characteristics of residual stress before and after ultrasonic impact and the influence law of residual stress by changing the needle moving speed were analyzed , aiming to study the effect of ultrasonic impact using on residual stress of 7A52 aluminum alloy joint. The simulation results show that the ultrasonic impact treatment could significantly improve the surface residual stress of weld seam and heat-affected zone , and the compressive stress in welded joint decreased with the increase of impact moving speed.

Key words: ultrasonic impact; residual stress; numerical